Transformation between 2D and 3D Covalent Organic Frameworks via Reversible [2+2] Cycloaddition

Thaksen Jadhav,‡ Yuan Fang,‡ Chenghao Liu,‡ Afshin Dadvand, Ehsan Hamzehpoor, William Patterson, Antranik Jonderian, Robin S. Stein, Dmitrii F. Perepichka*

Department of Chemistry, McGill University, 801 Sherbrooke Street West, Montreal, Quebec H3A 0B8, Canada.

Supporting Information Placeholder

ABSTRACT: We report the first transformation between crystalline vinylene-linked two-dimensional (2D) polymers and crystalline cyclobutane-linked three-dimensional (3D) polymers. Specifically, absorption-edge irradiation of the 2D poly(arylenevinylene) covalent organic frameworks (COFs) results in topological [2+2] cycloaddition cross-linking the π-stacked layers in 3D COFs. The reaction is reversible and heating to 200°C leads to a cycloreversion while retaining the COF crystallinity. The resulting difference in connectivity is manifested in the change of mechanical and electronic properties, including exfoliation, blue-shifted UV-Vis absorption, altered luminescence, modified band structure and different acid-doping behavior. The Li-impregnated 2D and 3D COFs show a significant ion conductivity of 1.8×10^{-4} S/cm and 3.5×10^{-5} S/cm, respectively. Even higher room temperature proton conductivity of 1.7×10^{-2} S/cm and 2.2×10^{-3} S/cm was found for H_2SO_4-treated 2D and 3D COFs, respectively.

1. INTRODUCTION

Cross-linking of polymers has been used for more than a century in the vulcanization of rubber, and it is the key process in the formulation of adhesives and structural materials, lithographic micro/nanofabrication,[1-4] 3D printing[5-6] and many other applications. The new covalent bonds created during cross-linking can improve the mechanical strength, change glass transition temperature and solubility of the polymer.[7] Cycloaddition reactions of olefin containing polymers are of particular interest because of their reversibility, which creates new opportunities for self-healing plastics[8] and dynamic materials.[9-10] In the majority of cases, cross-linking is a random process transforming coiled polymer chains in an amorphous 3D solid. However, there are also examples where supramolecular self-assembly of the reactive groups in the solid-state enables a topological reaction whereby the order of the precursor defines the structure of the (cross-linked) product. Wegner's 1,4-addition polymerization of diacetylenes is a signature solid-state topological reaction that can produce single crystals of poly(diacetylene) upon irradiation of monomer crystals.[11-12] Related topological 1,4- and 1,6-addition polymerizations have been observed in crystals of oligoene monomers.[13-14]

Crystal engineering approaches[15-18] have been used to direct the assembly of diarylvinylene monomers to facilitate the solid-state [2+2] photodimerization. Furthermore, Schlutter and King groups used [2+2], [2+4] and [4+4] cycloaddition to cross-link crystals of multidentate small molecules into 2D polymer crystals.[19-21] Finally, polymerization in an single-crystal-to-single-crystal manner was achieved successfully via [2+2] cycloaddition using some coordination polymers and metal-organic frameworks.[22-29]

In the field of covalent organic frameworks (COFs),[30-40] the only reversible topological reaction reported to date is based on [4+4] cycloaddition from Jiang's group.[41] The packing of their boronate ester-linked 2D COF places the reactive anthracene moieties one on top of another, at a favorable distance of 3.4 Å, such that photoirradiation leads to their dimerization through 9,10-positions, resulting in a 2D COF with twinned layers. The reverse reaction is facilitated by rearomatization of the anthracene rings, and the original COF can be regenerated upon heating to 200°C. The only 2D to 3D transformation in COFs was recently reported by Thomas and co-workers, based on the [2+2] cycloaddition of 2D poly(arylene vinylene) COFs.[37] However, the resulting cross-linked product was amorphous, and no reversibility of this transformation was established. Finally, [2+2] cycloaddition in a solution of tetradentate styrylpyridinium monomers pre-assembled via catenation with cucurbit[8]uril was recently reported to result in 3D cyclobutane-linked COFs.[42]

Here we report the first topological polymerization that transforms π-stacked 2D poly(arylenevinylene)[34-37] sheets into fully covalent, cyclobutane-linked 3D *crystalline* porous solids. The transformation is achieved by light-induced [2+2] cycloaddition of vinylene-linked phenylenevinylene (**P^{2}PV**) and naphthalene vinylene (**P^{2}NV**) 2D COFs delivering phenylene cyclobutylene (**P^{3}PcB**) and naphthalene cyclobutylene (**P^{3}NcB**) 3D COF (Scheme 1). This cross-linking of COF layers can be reversed by heating the COFs at 200 °C, resulting in the opening of the strained cyclobutane rings and restoring the original poly(arylenevinylene) network. Using density functional theory (DFT) calculations, we show how this transformation affects the COF electronic

structure and probe the induced differences via optical (absorption, luminescence) spectroscopy and acid doping measurements. We further elucidate the effect of 2D-to-3D transformation on gas adsorption, exfoliation and ion (Li^+, H^+) transport properties of the COFs.

Scheme 1. Synthesis of P²PV and P²NV COFs,[36] their photoinduced [2+2] cycloaddition into P³PcB and P³NcB and thermal cycloreversion.[a]

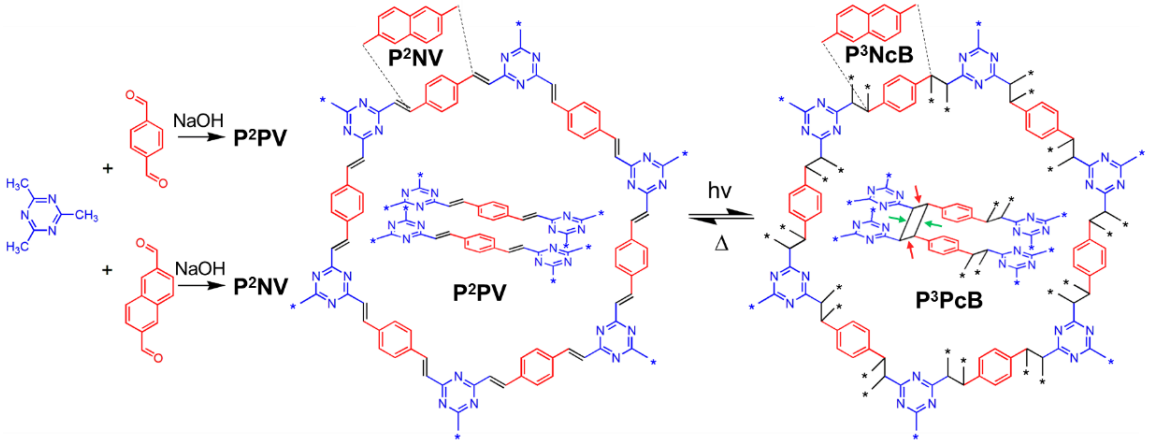

[a] Green arrows point to the 'new' bonds in the cyclobutane link (breaking of which leads to reverse reaction) and red arrows point to the single bond between triazine and phenyl rings (breaking of which leads to 'perforation' of the sheet structure upon sonication).

2. RESULTS AND DISCUSSION

The 2D vinylene-linked **P²PV** and **P²NV** were synthesized by base-catalyzed aldol condensation of trimethyltriazine with terephthaldehyde and naphthalene-2,6-dicarbaldehyde, respectively, as reported earlier.[36] The photosensitivity of the **P²PV** was serendipitously discovered as photobleaching upon prolonged daylight exposure. We hypothesized that the observed color change could be caused by a [2+2] cyclization of the adjacent vinylene bonds breaking the π-conjugation. To verify this hypothesis, we irradiated the stirred **P²PV** suspension in carefully degassed inert solvents and characterized the resulting product **P³PcB** by IR, ^{13}C NMR and Raman spectroscopy (Figures 1 and S1). The spectral data clearly shows the depletion of the vinylene links and formation of new cyclobutane rings: the intensity of C=C stretching (1631 cm^{-1}) in the IR spectra is suppressed and simultaneously a new peak appears at 2927 cm^{-1}, attributed to C-H stretching of cyclobutane rings (

Figure **1**a). The decreasing intensity of C=C vibration intensity upon photoirradiation is also seen in the Raman spectra (Figure S1). To aid the characterization of the cyclized COFs, we also synthesized the corresponding reference compounds 2,4,6-tristyryltriazine (TST) and studied spectroscopically its photocyclization (Figure S2-4). The ^{13}C NMR of **P³PcB** shows a new peak at 44 ppm, the expected chemical shift of cyclobutane' carbons (

Figure **1**b).[25] At the same time, a significant decrease in the ~136 ppm peak supports the disappearance of the vinylene carbons. Along with that, the triazine carbon signal shifts from 169 ppm (**P²PV**) to 175 ppm (**P³PcB**). Similar spectroscopic changes have also been observed upon photocyclization of **P²PN** into **P³PcN** (Figure S5).

Powder X-ray diffraction (PXRD) analysis of **P²PV** and **P³PcB** reveals resembling crystal structures, as expected for a topological transformation (Figure 2a,b). The (hk0) diffractions at 2θ = 4.9° (100), 8.4° (110), 9.7°(200), and 12.8° (210) shift upon photocyclization to a slightly higher angle, to 2θ =5.0°, 8.6°, 9.9°, and 13.1°. On the hand, the broad reflection at 2θ =~27° in **P²PV** corresponding to the π-stacking of 2D sheets with an interlayer distance of 3.4 Å, is replaced with a new peak at 2θ =18.2°, assigned to (002) reflection, conveying an increase of the interlayer spacing to 4.9 Å. The sharper and more intense appearance of this new peak signifies a higher degree of crystallographic order in the c-direction, consistent with the cross-linking along this direction. The crystallinity is also preserved upon cyclization of **P²NV** and accompanied by a slight shift of its (100) reflection from 4.2° to 4.4° in **P³NcB** (Figure 2c,d). A similar emergence of the (002) peak at 2θ =18.1° also manifests its improved order along the cross-linking direction.

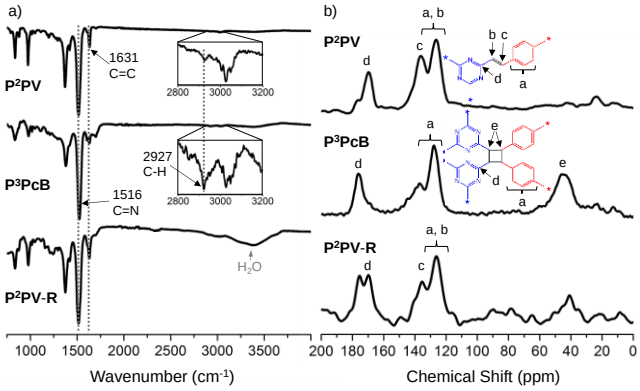

Figure 1. Comparison of the IR (a) ^{13}C cross-polarization magic angle spinning NMR spectra (b) of **P²PV**, **P³PcB** and **P²PV-R**.

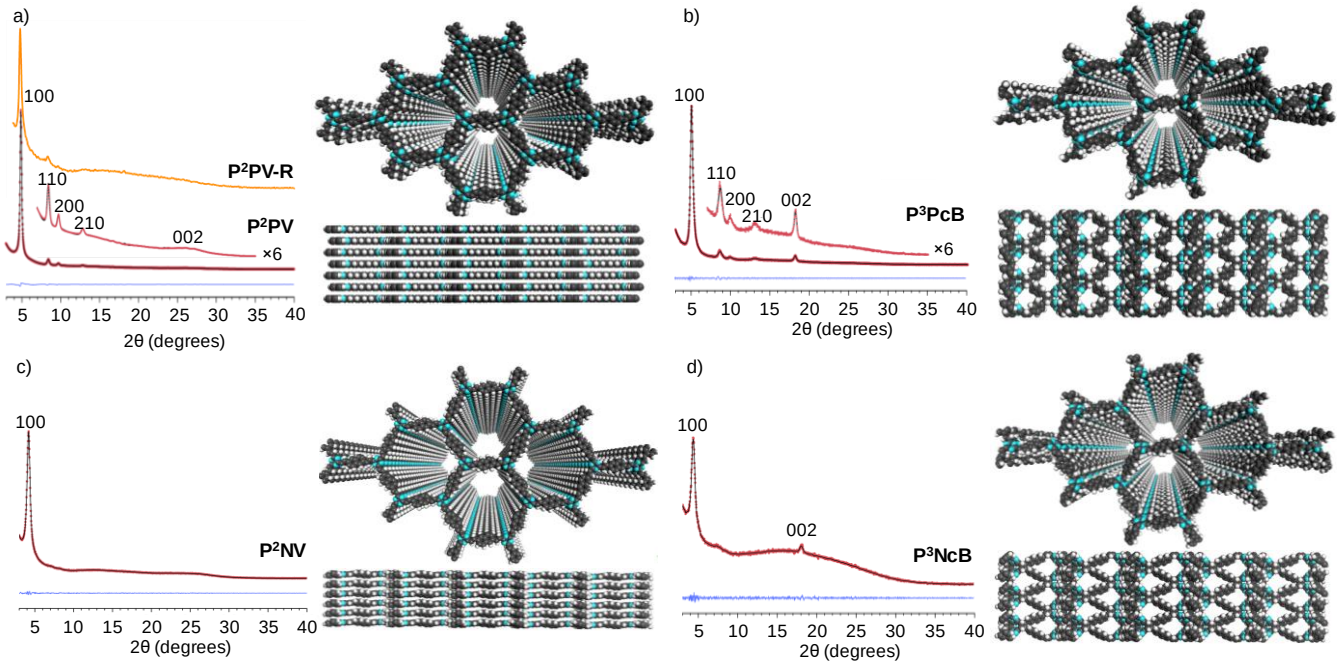

Figure 2. PXRD patterns (red dots) of (a) **P²PV**, (b) **P³PcB**, (c) **P²NV** and (d) **P³NcB** with Pawley refinement (black line, residual in blue) and corresponding molecular models viewed from [001] (top) and [100] planes (bottom). The orange line in (a) shows PXRD pattern of cyclo-reversed **P²PV-R**.

Full profile Pawley refinement of the diffraction patterns for both **P²PV** and **P³PcB** indicates a hexagonal structure, with unit cell parameters $a = b = 21.3$ Å, $c = 6.9$ Å; $\alpha = \beta = 90°$, $\gamma = 120°$ for **P²PV** ($R_{wp} = 1.95\%$, $R_p = 1.55\%$) and $a = b = 20.3$ Å, $c = 9.8$ Å; $\alpha = \beta = 90°$, $\gamma = 120°$ for **P³PcB** ($R_{wp} = 2.93\%$, $R_p = 1.92\%$) (Figure 2a,b). The small observed in-plane contraction within the cross-linked 2D polymer sheets (vectors *a, b*) as well as the more significant out-of-plane expansion (vector *c*) are an expected result of the [2+2] cross-linking of the COF layers. These lattice changes are further supported by predictions of molecular modelling. Both restricted and unrestricted optimization using molecular mechanics reveal flat sheets in **P²PV** (unrestricted unit cell parameters $a = 22.3$ Å, $b = 22.1$ Å, $c = 6.6$ Å, $\alpha = 89.9°$, $\beta = 89.8°$, $\gamma = 119.7°$, Figure S13), while **P³PcB** is corrugated with out-of-plane zigzag deformation of the sheets. This corrugation shortens the *a*-/*b*-vectors and significantly extends the *c*-vector (unrestricted unit cell parameters $a = 20.5$ Å, $b = 20.6$ Å, $c = 8.4$ Å, $\alpha = 89.7°$, $\beta = 90.5°$, $\gamma = 67.9°$, Figure S14), as observed by PXRD.

Pawley refinement and molecular models of **P²NV** and **P³NcB** COFs featuring a slightly longer naphthalene linker reveal the same structural changes (Figure 2c,d). The unit cell of **P²NV** ($a = b = 26.6$ Å, $c = 3.5$ Å; $\alpha = \beta = 90°$, $\gamma = 120°$; $R_p = 1.45\%$, $R_{wp} = 2.00\%$) undergoes similar in-plane contraction and out-of-plane expansion upon its cross-linking into **P³NcB** ($a = b = 24.5$ Å, $c = 9.9$ Å; $\alpha = \beta = 90°$, $\gamma = 120°$; $R_p = 1.53\%$, $R_{wp} = 2.02\%$). Further discussion is provided in the SI.

The degree of cyclization, as well as the crystallinity of the formed, 3D COF depend critically on the environment. In fact, the recently reported [2+2] cyclization of the same COF in ethanol dispersion produced an amorphous product.[37] We have investigated the cyclization of **P²PV** in various environments and founds that low-to-medium polarity aprotic media (hexane and its mixtures with toluene and acetonitrile) result in crystalline **P³PcB** while using polar protic solvents (water, methanol) as a dispersion medium invariably leads to low crystalline or amorphous products (Figure S6). This is likely connected to small changes in the interlayer packing brought about by hydrogen bonding of the triazine ring in protic solvents that affects the proximity of the reactive vinylene groups. Indeed, upon contact with water, **P²PV** shows a multifold expansion in volume, a 0.4° shift of the (100) peak and intensification of the (1*k*0) peaks in its PXRD pattern,[36] while there is only a small shift in PXRD (0.16°) and no change in the COF volume when immersed in hexane (Figure S7). We also note that the highest crystallinity in the **P³PcB** COF was achieved via absorption-edge irradiation method using a halogen lamp, while UV-induced cyclization leads to a decrease or loss of crystallinity (Figure S8). The deeper penetration depth of the higher wavelength light is thought to result in a more homogeneous photocyclization reducing the local strain in the COF crystal.

The effect of cyclization on the COF porosity was studied by Brunauer–Emmett–Teller (BET) method using N_2 adsorption at 77 K. The cyclization of **P²PV** results in a slight increase of porosity, from 880 m^2/g to 1037 m^2/g for **P³PcB** (Figure 3a and Figure S15),[43] which might be attributed to better accessibility of the pores due to their 3D connectivity. Pore distribution analysis shows that the previously observed for **P²PV** ~11 Å pores[36] are preserved during its transformation into **P³PcB**, but also a new population of pores with a diameter of ~6.5 Å appears (Figure 3b). The

latter is in agreement with a new channel perpendicular to the cross-linking direction created after cyclization, as shown in the lower molecular model in Figure 2b. As further evidence of cross-linking, the dynamic behavior manifested in pronounced swelling experienced by **P²PV** upon contact with water,[36] was not observed for **P³PcB**.

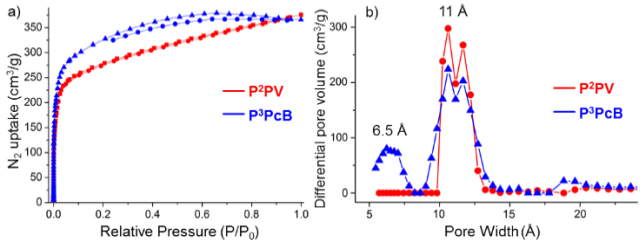

Figure 3. (a) N_2 adsorption/desorption isotherms and (b) the pore size distribution profiles of **P²PV** and **P³PcB**.

Change in connectivity was validated by exfoliation of **P²PV** and **P³PcB** as performed by stirring in concentrated H_2SO_4.[44] We speculated that electrostatic repulsion of positively charged sheets would facilitate exfoliation of protonated 2D COF **P²PV** but not of cross-linked 3D COF **P³PcB**. Indeed, drop-casting of the supernatant solution of protonated COF on TEM grids reveals large (5-10 μm) sheets for **P²PV** but not for **P³PcB** for which smaller (<1/2 μm) particles of higher thickness were observed (Figure 4a,b). The COFs appear stable after H_2SO_4 soaking, which is evident by IR spectroscopy (Figure S16). Forcing further exfoliation by ultrasonic agitation shows no apparent change to **P²PV** sheets (Figure S17), but such treatment of **P³PcB** COF particles leads to significant perforation with no observable sheet structure (Figure 4c). The latter behavior might be explained by sonication-induced cycloreversion of **P³PcB** in the 'wrong direction' (red arrows in Scheme 1), which could form diphenyl- and di(triazinyl)vinylene links and break the original 2D connectivity.

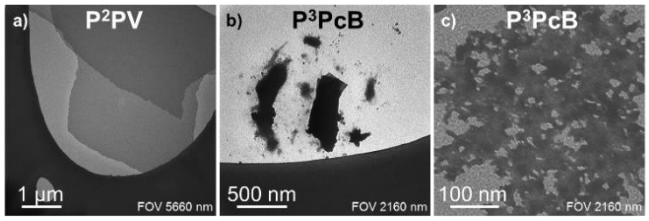

Figure 4. TEM images of exfoliated **P²PV** (a) and **P³PcB** (b) exfoliated by stirring in conc. H_2SO_4. (c) Further exfoliation by ultrasonication of **P³PcB** leads to its perforation.

The conversion of vinyl links to cyclobutane significantly affects its photophysical properties. The diffuse reflectance spectra of the yellow **P²PV** powder reveals an absorption edge at 500 nm, corresponding to the optical band gap E_g of 2.52 eV (Figure 5a). Upon photocyclization, the absorption edge of the resulting off-white **P³PcB** is blue-shifted to 420 nm (E_g = 2.95 eV), as expected due to the breaking of the π-conjugation at the cyclobutane links. A similar transformation has also been observed for the naphthalene-based **P²NV** COF (Figure 5c). The cyclization is accompanied by the blue shift of the fluorescence band for both **P²PV** and **P²PN** COFs (Figure 5b,d). The resulting **P³PcB** reveals a dramatically suppressed fluorescence due to poor emissivity of non-conjugated benzene and triazine moieties, as noted earlier.[37] Interestingly, the luminescence becomes more intense in the cyclized **P³PcN**, which we attribute to the isolated naphthalene luminophore, unaffected by exciton migration and quenching (as is the case for conjugated **P²PN**).

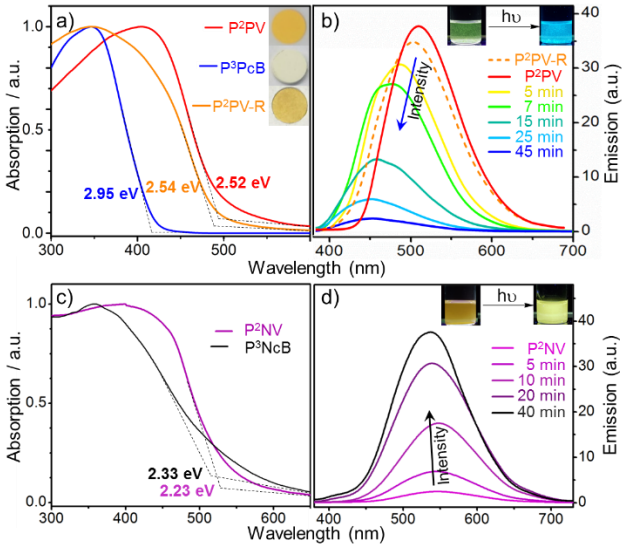

Figure 5. Diffuse reflectance spectra of **P²PV** (a, red) and **P²NV** (c, purple), its photocyclization products **P³PcB** (a, blue) and **P³NcB** (c, black) (halogen lamp irradiation) and cycloreversion product **P²PV-R** (a, orange) (heating at 200 °C); inset shows color of **P²PV**, **P³PcB** and **P²PV-R**. b and d) Evolution of fluorescence spectra of **P²PV** (b) and **P²NV** (d) upon irradiation by halogen lamp; insets shows photos of **P²PV** (b) and **P²NV** (d) suspension in hexanes before and after irradiation.

Band structures calculated with periodic DFT using a hybrid exchange-correlation functional (HSE06) shed further light on the cross-linking-induced changes of electronic properties. Cross-conjugation via meta-connected triazine units limits the band dispersion in **P²PV** monolayer (Figure 6a). The valence band with its maximum (VBM) at -5.72 eV is almost flat (dispersion= 0.05 eV), as could be expected based on the nodes of the HOMO (Figure S21). The conduction band with its minimum (CBM) at -2.93 eV is represented by a combination of a pair of Dirac bands (dispersion = 0.25 eV) and a completely flat band, expected for the Kagome-honeycomb 2D lattice.[45-47] This band structure points to potential interesting topological electronic effects in n-doped state of **P²PV**. The predicted direct (Γ-Γ) bandgap of 2.79 eV is slightly larger than the experimental optical gap (2.52 eV) of the bulk COF, likely due to interlayer π-π interactions in the latter. Indeed, DFT predicts a substantial dispersion (1.40 eV for HOVB and 1.55 eV for LUCB) of both bands upon AA stacking of **P²PV** sheets (Figure S20), although the extent of this effect in the bulk COF will depend on the exact registry of the stacking. Cyclization of **P²PV** to

P³PcB introduces an indirect (L-Γ) bandgap that is significantly increased to 3.51 eV (Figure 6b), raising CBM to -2.74 eV and lowering VBM to -6.24 eV. This is accompanied by an expected flattening of both valence and conduction bands (dispersion = 0.04 eV for HOVB and 0.11 eV for LUCB) due to the breaking of π-conjugation, predicting an electrically insulating behavior.

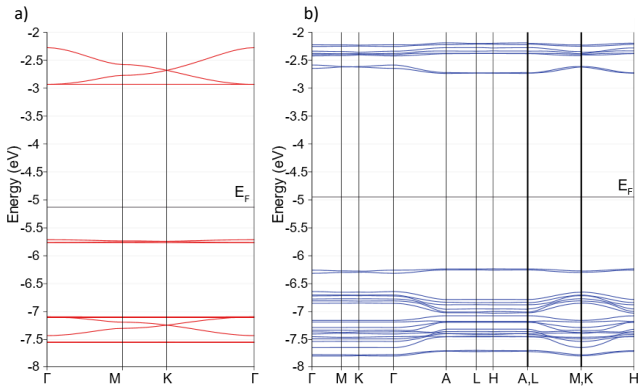

Figure 6. DFT-calculated band structure of monolayer **P²PV** (a), and **P³PcB** (b).

The different electronic structure of π-conjugated **P²PV** and non-conjugated **P³PcB** is further revealed by the effect of acid doping. Adding concentrated H_2SO_4 transforms the yellow **P²PV** to a completely black material with the absorption edge in the NIR region (E_g = 1.70 eV, Figure 7). This can be attributed to the enhanced donor-acceptor interactions between electron-rich phenylene vinylene and electron-deficient protonated triazine moiety. Such a dramatic red-shift is suppressed in the non-conjugated **P³PcB,** although the residual red color reveals the presence of incompletely cyclized fragments. Indeed, the absorption shoulder of the protonated **P³PcB** at ~550 nm is very similar to the absorption of the H_2SO_4 solution of TST. The protonation of both COFs is completely reversible and neutralization with ammonia restores the original absorption and visual appearance of the material (yellow for **P²PV**, white for **P³PcB**). Similar acid-induced optical switching has been previously observed in other COFs with triazine[48-49] and perylene[35] nodes.

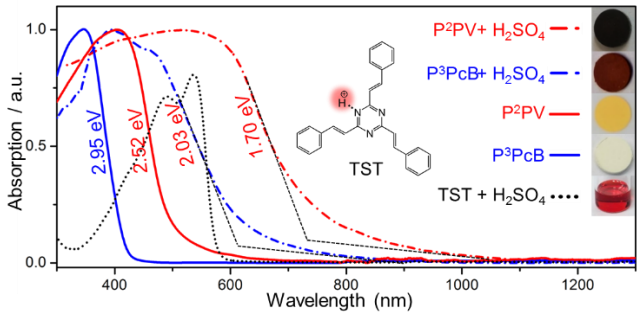

Figure 7. Comparison of diffuse reflectance spectra of H_2SO_4 doped **P²PV** and **P³PcB** with the pristine COF spectra and solution absorption of 2,4,6-tri((E)-styryl)-1,3,5-triazine (TST) in H_2SO_4. The inset shows photos of the acid-doped materials.

Although [2+2] photocycloaddition reactions are well-established, the solid-state cleavage of cyclobutane ring preserving the crystallinity is relatively rare.[25, 50] We demonstrate that, after heating **P³PcB** suspension in mesitylene at 200 °C in a pressurized tube for 2 days, the yellow color and the corresponding absorption band in the visible range are restored (Figure 5a). The IR spectra of thus produced **P²PV-R** showed a reduction of the sp^3 C-H stretching at 2927 cm^{-1} and regain of the C=C stretch at 1631 cm^{-1} (

Figure **1**). Photoluminescence spectra (Figure 5b) show that the resulting **P²PV-R** powder recovers the original yellow fluorescence. The PXRD pattern (Figure 2a) further demonstrates the restoration of the original **P²PV** peak positions. To the best of our knowledge, this is the first reported *reversible* transformation of a COF between 2D and 3D topology, preserving the overall crystallinity.

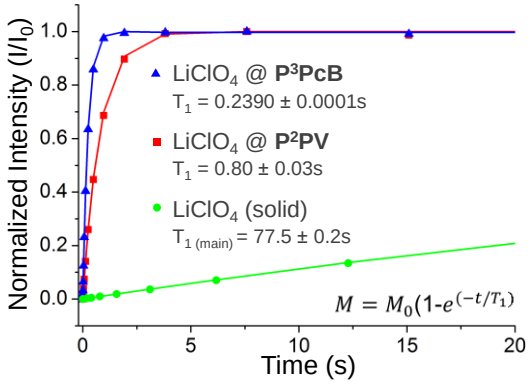

Figure 8. Saturation recovery plot from ^{7}Li ssNMR spectra (10 kHz, magic angle spinning) of **P²PV** and **P³PcB** impregnated with $LiClO_4$ (30% w/w) and $LiClO_4$ solid at ~40% relative humidity. T_1 relaxation time constant reveals the differences in mobility of the ^{7}Li ions. Full saturation recovery plot of $LiClO_4$ is shown in Figure S25.

Uniform 1D channels decorated with nitrogen atoms (Lewis bases) are of potential interest for solid electrolytes, and lithium ion conductivity of COFs has already become a topic of significant interest. Various strategies including incorporation of functional groups and ionic moieties have been explored to improve the ion conductivity and Li transfer ratio,[51-54], and Li conductivity as high as 7×10^{-3} S/cm has been achieved in a COF with lithium benzimidazolate linkers (at room temperature, with ~20 wt % added propylene carbonate).[52] We note, however, that hydrolytic instability of the C=N and B–O linkers used in these COFs may limit potential applications.

First, the mobility of lithium ions within the COFs was evaluated using NMR saturation recovery experiments[51] (Figure 8). The spin–lattice relaxation times were determined to be T_1 = 0.24 and 0.80 s for $LiClO_4$-impregnated

P²PV and **P³PcB**, respectively, measured at a relative humidity (RH) of ~40%. These values are several orders magnitude faster than in $LiClO_4$ hydrate (T_1 = 77.5 ± 0.2 s at ~40% RH; even longer recovery time ~2.5×10^3 s was reported[51] for anhydrous $LiClO_4$) and are among the fastest reported for Li-impregnated COFs.[51, 53]

The lithium ion conductivity of **P²PV** and **P³PcB** COFs was measured using electrochemical impedance spectroscopy on compressed pellets impregnated with $LiClO_4$ (30% w/w), at room temperature (297 K) and RH of ~40%. The fit of the Nyquist plots reveals a notable room-temperature ionic conductivity of ~1.8×10^{-4} S/cm and ~3.5×10^{-5} S/cm for **P²PV** and **P³PcB**, respectively (Figure 9a). These values compare favorably to the classical solid polymer electrolytes such as $LiClO_4$:PEO (~10^{-5} S/cm at room temperature).[55] We note, however, that the conductivity drops dramatically after vacuum drying the COF pellets (0.02 mbar, 65 °C). This behavior points to the possible role of the trapped water molecules in assisting the Li ion mobility, which is an obvious problem for the potential application in batteries. On the other hand, wetting the dried pellets with a drop of anhydrous dimethylcarbonate inside the glovebox fully restores the ion conductivity: ~1.7×10^{-4} S/cm for **P²PV** and ~1.1×10^{-4} S/cm for **P³PcB** (Figure 9b). Temperature-dependent measurements for **P²PV** and **P³PcB** reveals the raise of ion conductivity to 1.3×10^{-3} S/cm and 7.5×10^{-4} S/cm at 75 °C, with a similar activation energy of 0.37 eV and 0.35 eV, respectively (Figure 9c). The electron conductivity of Li-free vacuum-dried COFs is negligible (<1×10^{-9} S/cm), as expected based on their band structure. These results suggest these COFs could be viable as solid electrolytes for batteries.

There has also been a significant interest in proton-conducting COFs.[56-61] While proton conductivity of ~10^{-1} S/cm can be achieved in commercial Nafion films (the benchmark proton conductor), it requires elevated temperature, ca. 60 – 80 °C and high RH ~98 %.[62-63] On the other hand, comparable proton conductivity of up to 1.1×10^{-1} S/cm at 80°C (5.5×10^{-2} S/cm at 293 K and 98% RH) can be achieved H_3PO_4 treated (imine-linked) COFs, which paves the way for COFs application in fuel cells.[64]

We employed impedance analysis to evaluate the proton conductivity of H_2SO_4-treated **P²PV** and **P³PcB** at RH of 75%. The samples were soaked in 50% H_2SO_4 solution in acetonitrile for 10 min then washed with acetonitrile to remove an excess of acid, vacuum dried and pressed into pellets, and held in a desiccator above saturated NaCl(aq) (RH = 75%) for 24 h before the measurement. Nyquist plots of thus treated pellets exhibited proton conductivity of 1.7×10^{-2} S/cm (**P²PV**) and 2.2×10^{-3} S/cm (**P³PcB**) at 294 K (Figure 9d). The former value is among the highest reported for COFs at room temperature and is the first example of proton-conducting COF with hydrolytically stable vinylene (CH=CH) links. As with Li ion conductivity, transforming the π-conjugated 2D COF into 3D COF leads to a moderate but consistent decrease of the proton conductivity, which may be attributed to the misalignment of triazine lone pairs upon photo-crosslinking.

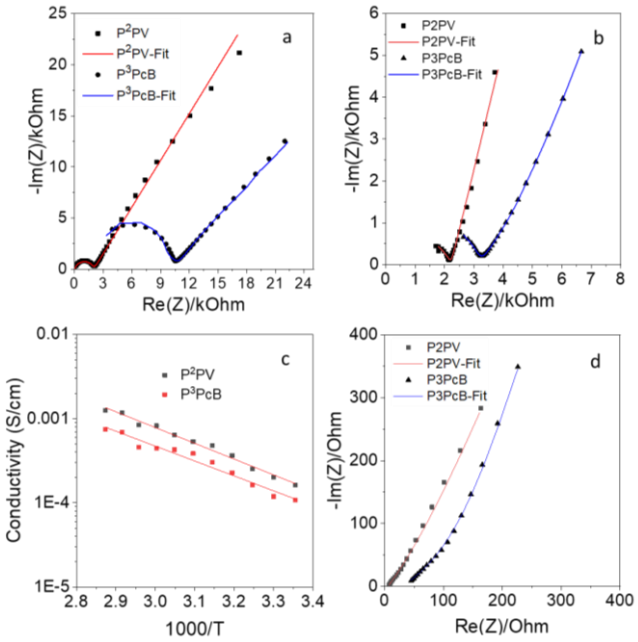

Figure 9. Nyquist plot and associated fits of **P²PV** (red) and **P³PcB** (blue) pellets impregnated with $LiClO_4$ at (a) 40% RH and (b) vacuum-dried and wetted with dimethyl carbonate. c) Arrhenius plot of the temperature-dependent Li-ion conductivity. d) Nyquist plot and associated fits of H_2SO_4-treated **P²PV** and **P³PcB** (40% RH). All measurements carried in 1 MHz to 1 Hz frequency range, with an oscillating voltage of 50 mV.

3. CONCLUSIONS

We have shown that photo-irradiation of 2D poly(arylene vinylene) COFs results in a [2+2] cycloaddition reaction which cross-links the COF sheets, affording new poly(arylene cyclobutylene) as a porous solid with 3D covalency. The products (3D COFs) loose the characteristic yellow color of the reactants (2D COFs) but retain their crystalline order. The reaction is reversible, and the thermal opening of cyclobutane ring at 200 °C regenerates the initial yellow 2D COF. This COF-to-COF transformation is topological and is perturbed by the presence of protic solvents, likely due to misalignment of the reactive vinylene groups; we also note that such transformation is generally ineffective in analogous 1D poly(phenylene vinylene)s. The photocyclization changes the electronic structure of the COFs. The 'flattening' of the conductance band (semiconductor-to-insulator transition) and band-gap increase are predicted by DFT band-structure calculations and confirmed by optical absorption measurement. Interestingly, photocyclization of the phenylene-linked **P²PV** is accompanied by the decrease of the COF fluorescence intensity whereas the same transformation in the naphthalene-linked **P²NV** leads to enhanced emission.

High lithium (1.8×10^{-4} S/cm) and proton (1.7×10^{-2} S/cm) conductivity at room temperature were achieved for the 2D **P²PV** doped with $LiClO_4$ and H_2SO_4, respectively. Its photo-

cyclization into 3D **P³PcB** results in ~5 times lower ion conductivity, possibly due to the misalignment of the basic nitrogen atoms in the COF pores.

While the observed photoresponsive nature of vinylene (CH=CH) linked 2D COFs and the access to all C-C linked 3D COFs is interest for multiple applications, its effect on the stability of such π-conjugated COFs as photoconductors should also be considered, e.g. in the context of water splitting applications.[35]

ASSOCIATED CONTENT

Supporting Information. The Supporting Information is available free of charge on the ACS Publications website: the PDF file containing experimental procedures for synthesis, transformation and characterization of COFs; computational protocols, conductivity, PXRD data, ^{13}C solid-state NMR spectra, BET sorption isotherms, additional TEM images, and fluorescence spectra.

AUTHOR INFORMATION

Corresponding Author

* dmitrii.perepichka@mcgill.ca

Author Contributions

‡These authors contributed equally.

ACKNOWLEDGMENT

This work was supported by US Army Office for Scientific Research (grant W911NF-17-1-0126) and NSERC of Canada. T.J. acknowledges FQRNT PBEEE international post-doctoral fellowship. Y.F. acknowledges NSERC and FQRNT post-doctoral fellowships. We thank T. Borchers (McGill University) for help with Raman measurements.

REFERENCES

1. Cai, J.; Zhu, Z.; Alkemade, P. F. A.; van Veldhoven, E.; Wang, Q.; Ge, H.; Rodrigues, S. P.; Cai, W.; Li, W.-D., 3D Volumetric Energy Deposition of Focused Helium Ion Beam Lithography: Visualization, Modeling, and Applications in Nanofabrication. *Adv. Mater. Interfaces* **2018,** *5*, 1800203.
2. Ji, S. X.; Wan, L.; Liu, C. C.; Nealey, P. F., Directed Self-Assembly of Block Copolymers on Chemical Patterns: A Platform for Nanofabrication. *Prog. Polym. Sci.* **2016,** *54-55*, 76-127.
3. Kim, M.; Ha, D.; Kim, T., Cracking-Assisted Photolithography for Mixed-Scale Patterning and Nanofluidic Applications. *Nat. Commun.* **2015,** *6*, 6247.
4. del Campo, A.; Arzt, E., Fabrication Approaches for Generating Complex Micro- and Nanopatterns on Polymeric Surfaces. *Chem. Rev.* **2008,** *108*, 911-945.
5. Eckel, Z. C.; Zhou, C. Y.; Martin, J. H.; Jacobsen, A. J.; Carter, W. B.; Schaedler, T. A., Additive Manufacturing of Polymer-Derived Ceramics. *Science* **2016,** *351*, 58-62.
6. Ligon, S. C.; Liska, R.; Stampfl, J.; Gurr, M.; Mülhaupt, R., Polymers for 3D Printing and Customized Additive Manufacturing. *Chem. Rev.* **2017,** *117*, 10212-10290.
7. Decker, C., Photoinitiated Crosslinking Polymerisation. *Prog. Polym. Sci.* **1996,** *21*, 593-650.
8. Chen, X.; Dam, M. A.; Ono, K.; Mal, A.; Shen, H.; Nutt, S. R.; Sheran, K.; Wudl, F., A Thermally Re-mendable Cross-Linked Polymeric Material. *Science* **2002,** *295*, 1698-1702.
9. Lu, Y.-X.; Guan, Z., Olefin Metathesis for Effective Polymer Healing via Dynamic Exchange of Strong Carbon–Carbon Double Bonds. *J. Am. Chem. Soc.* **2012,** *134*, 14226-14231.
10. Lu, Y.-X.; Tournilhac, F.; Leibler, L.; Guan, Z., Making Insoluble Polymer Networks Malleable via Olefin Metathesis. *J. Am. Chem. Soc.* **2012,** *134*, 8424-8427.
11. Enkelmann, V.; Leyrer, R. J.; Schleier, G.; Wegner, G., Macroscopic Single Crystals of Polymers by Solid-State Polymerization: A Study of the Monomer to Polymer Phase Transformation of 1,6-Dicarbazolyl Hexadiyne. *J. Mater. Sci.* **1980,** *15*, 168-176.
12. Sun, A. W.; Lauher, J. W.; Goroff, N. S., Preparation of Poly(diiododiacetylene), an Ordered Conjugated Polymer of Carbon and Iodine. *Science* **2006,** *312*, 1030-1034.
13. Dou, L.; Zheng, Y.; Shen, X.; Wu, G.; Fields, K.; Hsu, W.-C.; Zhou, H.; Yang, Y.; Wudl, F., Single-Crystal Linear Polymers Through Visible Light-Triggered Topochemical Quantitative Polymerization. *Science* **2014,** *343*, 272-277.
14. Itoh, T.; Nomura, S.; Uno, T.; Kubo, M.; Sada, K.; Miyata, M., Topochemical Polymerization of 7,7,8,8-Tetrakis(methoxycarbonyl)quinodimethane. *Angew. Chem., Int. Ed.* **2002,** *41*, 4306-4309.
15. Macgillivray, L. R.; Papaefstathiou, G. S.; Friscic, T.; Hamilton, T. D.; Bucar, D. K.; Chu, Q.; Varshney, D. B.; Georgiev, I. G., Supramolecular Control of Reactivity in the Solid State: From Templates to Ladderanes to Metal-Organic Frameworks. *Acc. Chem. Res.* **2008,** *41*, 280-291.
16. MacGillivray, L. R.; Reid, J. L.; Ripmeester, J. A., Supramolecular Control of Reactivity in the Solid State Using Linear Molecular Templates. *J. Am. Chem. Soc.* **2000,** *122*, 7817-7818.
17. Sinnwell, M. A.; MacGillivray, L. R., Halogen-Bond-Templated [2+2] Photodimerization in the Solid State: Directed Synthesis and Rare Self-Inclusion of a Halogenated Product. *Angew. Chem., Int. Ed.* **2016,** *128*, 3538-3541.
18. Papaefstathiou, G. S.; Zhong, Z. M.; Geng, L.; MacGillivray, L. R., Coordination-Driven Self-Assembly Directs a Single-Crystal-to-Single-Crystal Transformation that Exhibits Photocontrolled Fluorescence. *J. Am. Chem. Soc.* **2004,** *126*, 9158-9159.
19. Kissel, P.; Erni, R.; Schweizer, W. B.; Rossell, M. D.; King, B. T.; Bauer, T.; Gotzinger, S.; Schluter, A. D.; Sakamoto, J., A Two-Dimensional Polymer Prepared by Organic Synthesis. *Nat. Chem.* **2012,** *4*, 287-291.
20. Kissel, P.; Murray, D. J.; Wulftange, W. J.; Catalano, V. J.; King, B. T., A Nanoporous Two-Dimensional Polymer by Single-Crystal-to-Single-Crystal Photopolymerization. *Nat. Chem.* **2014,** *6*, 774-778.
21. Lange, R. Z.; Hofer, G.; Weber, T.; Schluter, A. D., A Two-Dimensional Polymer Synthesized through Topochemical [2 + 2]-Cycloaddition on the Multigram Scale. *J. Am. Chem. Soc.* **2017,** *139*, 2053-2059.
22. Mir, M. H.; Koh, L. L.; Tan, G. K.; Vittal, J. J., Single-Crystal to Single-Crystal Photochemical Structural Transformations of Interpenetrated 3D Coordination Polymers by 2+2 Cycloaddition Reactions. *Angew. Chem., Int. Ed.* **2010,** *49*, 390-393.
23. Michaelides, A.; Skoulika, S.; Siskos, M. G., Photoreactive 3D Microporous Lanthanide MOFs: Formation of a Strained Ladderane in a Partial Single Crystal-to-Single Crystal Manner. *Chem. Commun.* **2011,** *47*, 7140-7142.
24. Medishetty, R.; Koh, L. L.; Kole, G. K.; Vittal, J. J., Solid-State Structural Transformations from 2D Interdigitated Layers to 3D Interpenetrated Structures. *Angew. Chem., Int. Ed.* **2011,** *50*, 10949-10952.
25. Park, I.-H.; Chanthapally, A.; Zhang, Z.; Lee, S. S.; Zaworotko, M. J.; Vittal, J. J., Metal–Organic Organopolymeric Hybrid Framework by Reversible [2+2] Cycloaddition Reaction. *Angew. Chem., Int. Ed.* **2014,** *53*, 414-419.
26. Park, I. H.; Medishetty, R.; Kim, J. Y.; Lee, S. S.; Vittal, J. J., Distortional Supramolecular Isomers of Polyrotaxane

Coordination Polymers: Photoreactivity and Sensing of Nitro Compounds. *Angew. Chem., Int. Ed.* **2014,** *53*, 5591-5595.

27. Park, I.-H.; Medishetty, R.; Lee, H.-H.; Mulijanto, C. E.; Quah, H. S.; Lee, S. S.; Vittal, J. J., Formation of a Syndiotactic Organic Polymer Inside a MOF by a [2+2] Photo-Polymerization Reaction. *Angew. Chem., Int. Ed.* **2015,** *54*, 7313-7317.

28. Li, W. X.; Gu, J. H.; Li, H. X.; Dai, M.; Young, D. J.; Li, H. Y.; Lang, J. P., Post-synthetic Modification of a Two-Dimensional Metal-Organic Framework via Photodimerization Enables Highly Selective Luminescent Sensing of Aluminum(III). *Inorg. Chem.* **2018,** *57*, 13453-13460.

29. Pahari, G.; Bhattacharya, B.; Reddy, C. M.; Ghoshal, D., A Reversible Photochemical Solid-State Transformation in an Interpenetrated 3D Metal-Organic Framework with Mechanical Softness. *Chem. Commun.* **2019,** *55*, 12515-12518.

30. Waller, P. J.; Gandara, F.; Yaghi, O. M., Chemistry of Covalent Organic Frameworks. *Acc. Chem. Res.* **2015,** *48*, 3053-3063.

31. Jin, E.; Asada, M.; Xu, Q.; Dalapati, S.; Addicoat, M. A.; Brady, M. A.; Xu, H.; Nakamura, T.; Heine, T.; Chen, Q.; Jiang, D., Two-Dimensional sp^2 Carbon-Conjugated Covalent Organic Frameworks. *Science* **2017,** *357*, 673-676.

32. Jin, E.; Li, J.; Geng, K.; Jiang, Q.; Xu, H.; Xu, Q.; Jiang, D., Designed Synthesis of Stable Light-Emitting Two-Dimensional sp^2 Carbon-Conjugated Covalent Organic Frameworks. *Nat. Commun.* **2018,** *9*, 4143.

33. Diercks, C. S.; Yaghi, O. M., The Atom, the Molecule, and the Covalent Organic Framework. *Science* **2017,** *355*, eaal1585.

34. Lyu, H.; Diercks, C. S.; Zhu, C.; Yaghi, O. M., Porous Crystalline Olefin-Linked Covalent Organic Frameworks. *J. Am. Chem. Soc.* **2019,** *141*, 6848-6852.

35. Wei, S.; Zhang, F.; Zhang, W.; Qiang, P.; Yu, K.; Fu, X.; Wu, D.; Bi, S.; Zhang, F., Semiconducting 2D Triazine-Cored Covalent Organic Frameworks with Unsubstituted Olefin Linkages. *J. Am. Chem. Soc.* **2019,** *141*, 14272-14279.

36. Jadhav, T.; Fang, Y.; Patterson, W.; Liu, C.-H.; Hamzehpoor, E.; Perepichka, D. F., 2D Poly(arylene vinylene) Covalent Organic Frameworks via Aldol Condensation of Trimethyltriazine. *Angew. Chem., Int. Ed.* **2019,** *58*, 13753-13757.

37. Acharjya, A.; Pachfule, P.; Roeser, J.; Schmitt, F.-J.; Thomas, A., Vinylene-Linked Covalent Organic Frameworks by Base-Catalyzed Aldol Condensation. *Angew. Chem., Int. Ed.* **2019,** *58*, 14865-14870.

38. Bi, S.; Yang, C.; Zhang, W.; Xu, J.; Liu, L.; Wu, D.; Wang, X.; Han, Y.; Liang, Q.; Zhang, F., Two-Dimensional Semiconducting Covalent Organic Frameworks via Condensation at Arylmethyl Carbon Atoms. *Nat. Commun.* **2019,** *10*, 2467.

39. Geng, K.; He, T.; Liu, R.; Tan, K. T.; Li, Z.; Tao, S.; Gong, Y.; Jiang, Q.; Jiang, D., Covalent Organic Frameworks: Design, Synthesis and Functions. *Chem. Rev.* **2020**, DOI: 10.1021/acs.chemrev.9b00550

40. Chen, X.; Geng, K.; Liu, R.; Tan, K. T.; Gong, Y.; Li, Z.; Tao, S.; Jiang, Q.; Jiang, D., Covalent Organic Frameworks: Chemical Approaches to Designer Structures and Built-In Functions. *Angew. Chem., Int. Ed.* **2020**, DOI:10.1002/anie.201904291.

41. Huang, N.; Ding, X.; Kim, J.; Ihee, H.; Jiang, D., A Photoresponsive Smart Covalent Organic Framework. *Angew. Chem., Int. Ed.* **2015,** *54*, 8704-8707.

42. Gao, Z.-Z.; Wang, Z.-K.; Wei, L.; Yin, G.; Tian, J.; Liu, C.-Z.; Wang, H.; Zhang, D.-W.; Zhang, Y.-B.; Li, X.; Liu, Y.; Li, Z.-T., Water-Soluble 3D Covalent Organic Framework that Displays an Enhanced Enrichment Effect of Photosensitizers and Catalysts for the Reduction of Protons to H_2. *ACS Appl. Mater. Inter.* **2020,** *12*, 1404-1411.

43. Note that there is some batch-to-batch variation in the measured surface area of COFs. Slightly higher maximum surface are were reported by us (41 [ref]) and others (34 [ref]) for P^2PV COF. The reported here change of surface area upon cross-linking was measured for the same sample.

44. Burke, D. W.; Sun, C.; Castano, I.; Flanders, N. C.; Evans, A. M.; Vitaku, E.; McLeod, D. C.; Lambeth, R. H.; Chen, L. X.; Gianneschi, N. C.; Dichtel, W. R., Acid Exfoliation of Imine-linked Covalent Organic Frameworks Enables Solution Processing into Crystalline Thin Films. *Angew. Chem., Int. Ed.* **2020**, DOI:10.1002/ange.201913975.

45. Lakshmi, V.; Liu, C.-H.; Rajeswara Rao, M.; Chen, Y.; Fang, Y.; Dadvand, A.; Hamzehpoor, E.; Sakai-Otsuka, Y.; Stein, R. S.; Perepichka, D. F., A Two-Dimensional Poly(azatriangulene) Covalent Organic Framework with Semiconducting and Paramagnetic States. *J. Am. Chem. Soc.* **2020,** *142*, 2155-2160.

46. Paavilainen, S.; Ropo, M.; Nieminen, J.; Akola, J.; Räsänen, E., Coexisting Honeycomb and Kagome Characteristics in the Electronic Band Structure of Molecular Graphene. *Nano Lett.* **2016,** *16*, 3519-3523.

47. Barreteau, C.; Ducastelle, F.; Mallah, T., A Bird's Eye View on the Flat and Conic Band World of the Honeycomb and Kagome Lattices: Towards an Understanding of 2D Metal-Organic Frameworks Electronic Structure. *J. Phys-Condens Mat.* **2017,** *29*.

48. Kulkarni, R.; Noda, Y.; Kumar Barange, D.; Kochergin, Y. S.; Lyu, P.; Balcarova, B.; Nachtigall, P.; Bojdys, M. J., Real-Time Optical and Electronic Sensing with a β-amino Enone Linked, Triazine-Containing 2D Covalent Organic Framework. *Nat. Commun.* **2019,** *10*, 3228.

49. Ascherl, L.; Evans, E. W.; Gorman, J.; Orsborne, S.; Bessinger, D.; Bein, T.; Friend, R. H.; Auras, F., Perylene-Based Covalent Organic Frameworks for Acid Vapor Sensing. *J. Am. Chem. Soc.* **2019,** *141*, 15693-15699.

50. Chanthapally, A.; Kole, G. K.; Qian, K.; Tan, G. K.; Gao, S.; Vittal, J. J., Thermal Cleavage of Cyclobutane Rings in Photodimerized Coordination-Polymeric Sheets. *Eur. J. Chem.* **2012,** *18*, 7869-7877.

51. Vazquez-Molina, D. A.; Mohammad-Pour, G. S.; Lee, C.; Logan, M. W.; Duan, X.; Harper, J. K.; Uribe-Romo, F. J., Mechanically Shaped Two-Dimensional Covalent Organic Frameworks Reveal Crystallographic Alignment and Fast Li-Ion Conductivity. *J. Am. Chem. Soc.* **2016,** *138*, 9767-70.

52. Hu, Y.; Dunlap, N.; Wan, S.; Lu, S.; Huang, S.; Sellinger, I.; Ortiz, M.; Jin, Y.; Lee, S.-h.; Zhang, W., Crystalline Lithium Imidazolate Covalent Organic Frameworks with High Li-Ion Conductivity. *J. Am. Chem. Soc.* **2019,** *141*, 7518-7525.

53. Jeong, K.; Park, S.; Jung, G. Y.; Kim, S. H.; Lee, Y.-H.; Kwak, S. K.; Lee, S.-Y., Solvent-Free, Single Lithium-Ion Conducting Covalent Organic Frameworks. *J. Am. Chem. Soc.* **2019,** *141*, 5880-5885.

54. Xu, Q.; Tao, S.; Jiang, Q.; Jiang, D., Ion Conduction in Polyelectrolyte Covalent Organic Frameworks. *J. Am. Chem. Soc.* **2018,** *140*, 7429-7432.

55. Michael, M. S.; Jacob, M. M. E.; Prabaharan, S. R. S.; Radhakrishna, S., Enhanced Lithium Ion Transport in PEO-Based Solid Polymer Electrolytes Employing a Novel Class of Plasticizers. *Solid State Ion.* **1997,** *98*, 167-174.

56. Chandra, S.; Kundu, T.; Kandambeth, S.; BabaRao, R.; Marathe, Y.; Kunjir, S. M.; Banerjee, R., Phosphoric Acid Loaded Azo (-N=N-) Based Covalent Organic Framework for Proton Conduction. *J. Am. Chem. Soc.* **2014,** *136*, 6570-6573.

57. Ma, H.; Liu, B.; Li, B.; Zhang, L.; Li, Y.-G.; Tan, H.-Q.; Zang, H.-Y.; Zhu, G., Cationic Covalent Organic Frameworks: A Simple Platform of Anionic Exchange for Porosity Tuning and Proton Conduction. *J. Am. Chem. Soc.* **2016,** *138*, 5897-5903.

58. Xu, H.; Tao, S.; Jiang, D., Proton Conduction in Crystalline and Porous Covalent Organic Frameworks. *Nat. Mater.* **2016,** *15*, 722-726.

59. Meng, X.; Wang, H.-N.; Song, S.-Y.; Zhang, H.-J., Proton-conducting crystalline porous materials. *Chem. Soc. Rev.* **2017,** *46*, 464-480.
60. Sasmal, H. S.; Aiyappa, H. B.; Bhange, S. N.; Karak, S.; Halder, A.; Kurungot, S.; Banerjee, R., Superprotonic Conductivity in Flexible Porous Covalent Organic Framework Membranes. *Angew. Chem., Int. Ed.* **2018,** *57*, 10894-10898.
61. Meng, Z.; Aykanat, A.; Mirica, K. A., Proton Conduction in 2D Aza-Fused Covalent Organic Frameworks. *Chem. Mater.* **2019,** *31*, 819-825.
62. Sone, Y., Proton Conductivity of Nafion 117 as Measured by a Four-Electrode AC Impedance Method. *J. Electrochem. Soc.* **1996,** *143*, 1254.
63. Hickner, M. A.; Ghassemi, H.; Kim, Y. S.; Einsla, B. R.; McGrath, J. E., Alternative Polymer Systems for Proton Exchange Membranes (PEMs). *Chem. Rev.* **2004,** *104*, 4587-4612.
64. Yang, Y.; He, X.; Zhang, P.; Andaloussi, Y. H.; Zhang, H.; Jiang, Z.; Chen, Y.; Ma, S.; Cheng, P.; Zhang, Z., Combined Intrinsic and Extrinsic Proton Conduction in Robust Covalent Organic Frameworks for Hydrogen Fuel Cell Applications. *Angew. Chem., Int. Ed.* **2020**, DOI:10.1002/ange.201913802.

TOC